Available online at www.sciencedirect.com

SciVerse ScienceDirect

journal homepage: www.elsevier.com/locate/he

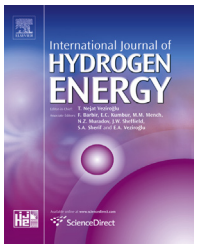

Structural characterization and electrochemical hydrogen storage properties of $Ti_{2-x}Zr_xNi$ ($x = 0$, 0.1, 0.2) alloys prepared by mechanical alloying

X.D. Li [a,*], O. Elkedim [a], M. Nowak [b], M. Jurczyk [b], R. Chassagnon [c]

[a] FEMTO-ST, MN2S, Université de Technologie de Belfort-Montbéliard, Site de Sévenans, 90010 Belfort cedex, France
[b] Institute of Materials Science and Engineering, Poznan University of Technology, Sklodowska-Curie 5 Sq., 60-965 Poznan, Poland
[c] Laboratoire Interdisciplinaire Carnot de Bourgogne, UMR 6303 CNRS, Université de Bourgogne, 9 Av. A. Savary, BP 47870, F-21078 Dijon, France

ARTICLE INFO

Article history:
Received 28 January 2013
Received in revised form
13 March 2013
Accepted 18 March 2013
Available online 15 April 2013

Keywords:
Ti_2Ni
Mechanical alloying
Electrochemical hydrogen storage properties
Zr substitution

ABSTRACT

Nominal Ti_2Ni was synthesized under argon atmosphere at room temperature using a planetary high-energy ball mill. The effect of milling time and Zr substitution for Ti on the microstructure was characterized by XRD, SEM and TEM, and the discharge capacities of $Ti_{2-x}Zr_xNi$ ($x = 0$, 0.1, 0.2) were examined by electrochemical measurements at galvanostatic conditions. XRD analysis shows that amorphous phase of Ti_2Ni can be elaborated by 60 h of milling, whereas Zr substitution hinders amorphization process of the system. The products of ball milling nominal $Ti_{2-x}Zr_xNi$ ($x = 0.1$, 0.2) were austenitic (Ti, Zr)Ni and partly TiO, despite the fact that the operation was carried out under argon atmosphere. By comparing the SEM micrographs, it is found that the amorphous phase of Ti_2Ni was formed in the stage of cold-welding during milling, while with Zr substitution particles were flaky and finer, inhomogeneous in size distribution with massive agglomeration. TEM analysis was carried out and confirmed the observations via XRD. In the electrochemical tests, amorphous Ti_2Ni shows the best discharge capacity at 102 mAh/g at a current density of 40 mA/g. Without need of activation, it exhibits extraordinary cycling stability under room temperature. On the other hand, the effect of Zr substitution on the electrochemical property of Ti_2Ni is tricky, as superficially the discharge capacity drops drastically with Zr substitution, but with increase of Zr content (from $x = 0.1$ to $x = 0.2$), the discharge capacity increases generally, which credits to larger unit-cell-volume provided by ZrNi compared to TiNi. It is also found that the Ti–Ni system becomes significantly susceptible to oxidation when Zr is introduced to the initial powders as mechanical alloying is deployed as a synthesis method.

1. Introduction

As a well-known shape memory alloy, binary Ti–Ni alloy has been studied extensively regarding its hydrogen storage properties [1,2]. Both TiNi and Ti_2Ni can be used as hydrogen carrier. It was first reported that hydride of Ti_2Ni ($Ti_2NiH_{2.9}$) had an electrochemical capacity of 500 mAh/g in a gaseous hydrogen absorption reaction [3]. Later the group of Luan

* *Corresponding author*. Tel.: +33 384583545.
E-mail addresses: xianda.li@utbm.fr, xianda.jake.li@gmail.com (X.D. Li).
0360-3199/$ – see front matter
http://dx.doi.org/10.1016/j.ijhydene.2013.03.098

et al. [4] prepared Ti_2Ni alloy by arc melting, but a mere 160 mAh/g discharge capacity was achieved with poor cycling stability. They concluded that the early capacity loss was due to the formation of irreversible $Ti_2NiH_{0.5}$. Most recently, amorphous Ti_2Ni alloy was investigated by Zhao et al. [5]. They found that amorphous phase of Ti_2Ni helps to stabilize cycling performance. In their experiment, the Ti_2Ni alloy was synthesized by solid-state sintering, and subsequent ball milling was carried out to obtain mainly an amorphous phase, which had a discharge capacity between 100 mAh/g and 125 mAh/g. On the other hand, non-milled Ti_2Ni (prepared solely by solid-state sintering) reached its highest capacity of 280 mAh/g in the first cycle, but dropped less than 100 mAh/g after 50 cycles.

There were also efforts regarding elemental substitution for Ti_2Ni alloy, such as $Ti_2Ni_{1-x}Al_x$, $Ti_2Ni_{1-x}B_x$ [6, 7], but the improvement was not satisfactory. Hiroyuki et al. [8] did a research on the hydrogenation properties of the ternary compound Ti_4Ni_2X (X = O, N, C). They found that these alloys all had higher hydrogen desorption pressure compared to Ti_2Ni, and presented a hydrogen pressure plateau. Lately, $(Ti_{1-x}V_x)_2Ni$ featuring a quasi-crystalline structure was studied [9]. The alloys were synthesized by arc melting and subsequent melt spinning. The discharge capacity reached 271.3 mAh/g when $x = 0.3$ and the cycling capacity retention rate were as good as approximately 80% after 30 cycles.

In respect of elemental substitution, Zr substitution for TiNi in order to improve the electrochemical properties is very active [10–13]. In the same element group with Ti, Zr substitution is quite a reasonable choice. It is reported that Zr is able to take the place of Ti in both austenitic and martensitic TiNi structure [10], and that ternary Ti–Zr–Ni alloys develop austenitic structure by melt spinning and martensitic structure by induction melting. The TiNi austenite has a cubic B2 CsCl-type structure (space group (SG) *Pm3m*) [14]. The TiNi martensite structure is monoclinic B19′ P21/m [15]. TiNi alloy that has an austenitic structure absorbs less hydrogen (1.5 H/AB) than TiNi with a martensitic structure (2.6 H/AB), and it does not present any plateau pressure when the hydrogen pressures are between 0.1 and 10 bar [16]. It is found that Zr substitution increases martensitic transformation (MT) temperature for TiNi, and on the other hand non-equilibrium technique such as melt-spinning decrease MT temperature. Therefore, Zr substitution may stabilize TiNi alloy in the austenitic phase at room temperature [17]. As for Ti_2Ni, Xiangyu Zhao et al. [5,18] have done a series of experiments for the preparation of Ti_2Ni. The procedure included sintering, ball milling, and annealing. Zr substitution was also implemented recently [19]. $Ti_{2-x}Zr_xNi$ (x = 0, 0.2, 0.4) were alloyed by solid-state sintering, followed by ball milling and subsequent annealing. They found Zr enhanced the discharge capacity of non-equilibrium at electrolyte temperatures of 313 K and 333 K. For example, $Ti_{1.6}Zr_{0.4}Ni$ had a stable discharge capacity of about 210 mAh/g at 313 K.

In this work, we have synthesized $Ti_{2-x}Zr_xNi$ ($x = 0, 0.1, 0.2$) from pure elemental powders using mechanical alloying. The microstructures and morphologies of the samples are analyzed by XRD, SEM and TEM to study the effect of milling time and Zr substitution. The cycle-life of the alloys as negative electrodes of Ni-MH batteries is presented.

2. Experimental

Commercial elemental powders of Ti (99.9% purity, particle size $\leq$ 150 μm, GoodFellow), Ni (99.5% purity, particle size $\leq$ 250 μm, GoodFellow) and Zr (particle size $\leq$ 45 μm, Goodfellow) were stoichiometrically loaded into stainless steel vials (volume 50 ml) with two stainless steel balls (diameter 20 mm) in a glove box filled with argon. 2 wt% alcohol was added as process control agent. The ball to powder weight ratio is 3.3. The milling was carried out in a planetary high-energy ball mill (Retsch PM 400) at 400 rpm under argon atmosphere at room temperature. For the purpose of dissipating heat that would otherwise give rise to high temperature, the milling was interrupted every 30 min.

The XRD patterns of $Ti_{2-x}Zr_xNi$ were analyzed by a Bruker D8 Advance X-ray diffractometer with Cu Kα radiation (λ = 0.15418 nm) filtered by nickel. The morphologies and microstructure of the powdered samples were characterized by scanning electron microscopy (SEM, JEOL JSM-5800LV) and transmission electron microscopy (TEM, JEOL JEM-2100 operating at 200 kV accelerating voltage).

Electrochemical properties were investigated using Multichannel Battery Interface ATLAS 0461. The working electrodes were prepared by compressing the milled powder and 10 wt% addition of Ni powder under a pressure of 326 MPa to form a small pellet between nickel nets acting as the current collector. The electrochemical properties of electrodes were measured in an H-type shape glass cell. $NiOOH/Ni(OH)_2$ was used as counter electrode to a cut-off potential of 0.7 V versus the reference electrode Hg/HgO. Before test, the electrodes were soaked in 6 M KOH electrolyte at room temperature after that they had been soaked in the same solution for 1 h at 100 °C.

3. Results and discussion

3.1. Microstructures

Fig. 1 shows the XRD patterns of Ti_2Ni as a function of milling time. To our knowledge, this is the first time that nominal Ti_2Ni is being mechanical alloyed from elemental powders. Comparing the patterns with the ones obtained by ball milling Ti_2Ni [19], the smooth peaks that appear in all samples at around 42° corresponds to Ti_2Ni phase. It can be seen that in Fig. 1(a), 20 h of milling has already yielded amorphous or nanocrystalline Ti_2Ni, leaving some residual element peaks in the meantime. The alloying is far from completion but the produced Ti_2Ni exhibits an amorphous/nanocrystalline form. After 40 h of milling, the main Ti_2Ni peak (42°) broadens even more while the intensity of element peaks decreases, indicating further amorphization process. When milling time reaches 60 h, the peak corresponding to Ti_2Ni becomes even smoother and element peaks disappear. This implies that the formation of amorphous Ti_2Ni has completed.

The XRD patterns of $Ti_{2-x}Zr_xNi$ ($x = 0, 0.1, 0.2$) mechanically alloyed 60 h is presented in Fig. 2. It is interesting to see that as Zr is introduced to the initial powders, the peaks in (b) (c) indicate crystalline phases. With further analysis, it is found

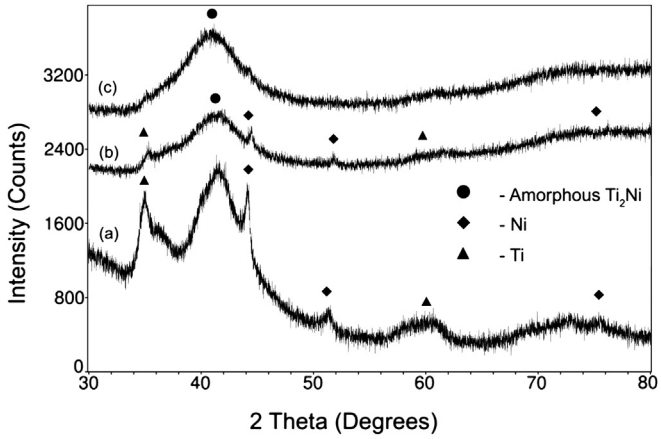

Fig. 1 – XRD patterns of mechanical alloying Ti_2Ni for different milling time: (a) 20 h, (b) 40 h, and (c) 60 h.

that the pattern consists of two main phases. One is ternary (Ti, Zr)Ni austenitic. It is reported in Ref. [20] that austenitic TiNi, a metastable phase at room temperature could be formed by ball milling. As shown in Fig. 2, peaks that correspond to (Ti, Zr)Ni shift slightly left to the ordinary TiNi austenitic pattern (PDF card 18-0899). This is the sign that Zr has replaced some Ti in the TiNi cubic structure, and an increase of lattice constant has taken place. That Zr substitution for Ti leads to cell-volume expansion was reported by Cuevas et al. [17]. The other phase was identified as TiO. Since the ratio of two initial elements Ti and Ni was 2:1, and because only pseudo binary Ti(Zr)Ni was formed, it is reasonable that the excess Ti had formed TiO. From using the XRD data, average crystallite sizes for samples with Zr were estimated at around 5 nm. It can be seen that Zr brought about two changes to the system. First, oxidation becomes severe when Zr is present. Similar result was also reported that additional Zr facilitates the oxidation for the amorphous Ti_2Ni alloy [19]. When ternary alloy Ti–Zr–Ni was heat treated under argon atmosphere, oxidation occurred in spite of the protective atmosphere. In our case, the oxidation took place during the milling process, when infiltration of air was possible due to fluctuation of temperature of the vial. Since every 30 min milling would be interrupted to prevent overheating, the temperature in the vials could rise and drop repeatedly. As a result, the air within the vials inflated and deflated. This is also supported by the sound of a gust of air when unloading vials from the valves, which implies the change of air pressure inside the vials. It should be noted that the oxidized element was Ti instead of Zr despite the fact that the electronegativity number of Ti is higher than Zr. The following reactions are deduced (be aware that oxygen and zirconium are relatively scarce while titanium is abundant):

$$Zr + O_2 \rightarrow ZrO_2 \quad (1)$$

$$Ti + Ni \rightarrow TiNi \quad (2)$$

$$Ti + ZrO_2 + TiNi \rightarrow 2TiO + ZrNi \quad (3)$$

Another change is that Zr obviously decreases the stability of amorphous Ti_2Ni. The mechanism of amorphization during mechanical milling is however of great complexity. There are two known models that seek to predict the possibility of formation of amorphous phase for two given elemental powders [21].

The possibility of forming amorphous phase for binary systems Ti–Ni and Ni–Zr is listed in Table 1. It can be seen that although the compositions of Ti–Ni in $Ti_{1.8}Zr_{0.2}Ni$ and $Ti_{1.9}Zr_{0.1}Ni$ are 60 Ti (at%) and 63 Ti (at%), which are in the range that Table 1 indicates (in both Miedema and CALPHAD models), the ratios of Ni–Zr do not fit (as Zr at% is 9). Furthermore, it is confirmed experimentally that additional Zr decreases the stability of amorphous Ti_2Ni [19].

Fig. 3 is the SEM micrographs of $Ti_{2-x}Zr_xNi$ that were milled 60 h. It can be seen that the morphologies changes greatly

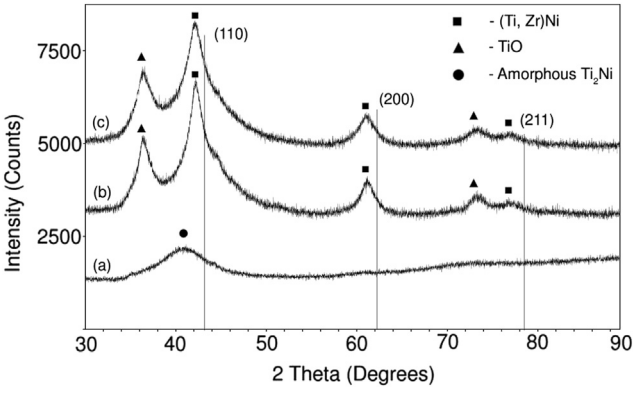

Fig. 2 – XRD pattern of $Ti_{2-x}Zr_xNi$ with a fixed milling time 60 h: (a) Ti_2Ni, (b) $Ti_{1.9}Zr_{0.1}Ni$, and (c) $Ti_{1.8}Zr_{0.2}Ni$.

Table 1 – Comparison of the predicted and observed glass-forming ranges in mechanically alloyed Ti–Zr–Ni.

System	Amorphous phase-forming range (at% solute)		
	Miedema model	CALPHAD	Observed
Ti–Ni	23–76Ti		28–72Ti
Ni–Zr	22–63Zr	17–67Zr	24–85Zr

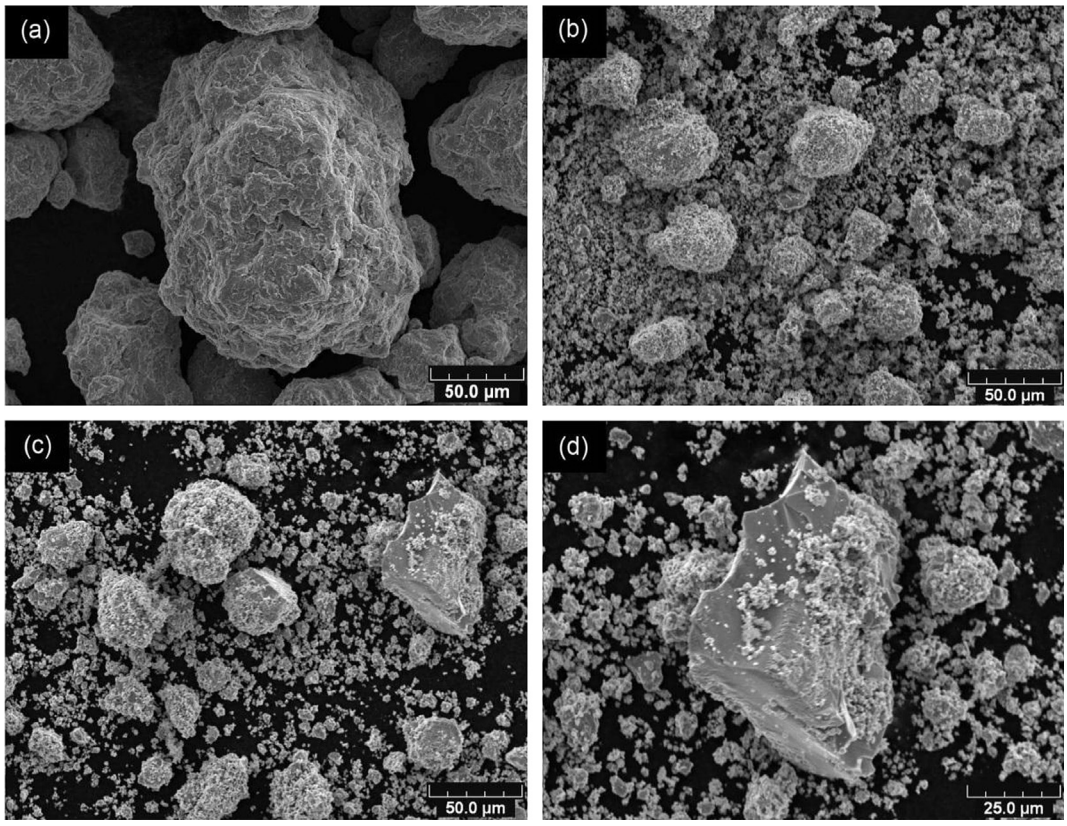

Fig. 3 – SEM micrographs of $Ti_{2-x}Zr_xNi$ milled 60 h: (a) $x = 0$, (b) $x = 0.1$, (c) $x = 0.2 \times 500$, and (d) $x = 0.2 \times 1000$.

with increase of Zr content. All the samples that show in Fig. 3 are milled 60 h, but as Zr has an effect of slowing down the amorphization process, the morphologies of (a), (b), (c) appear to be in the different stages of milling (chronologically backward). It is known that milling involves two major processes, namely cold-welding and fracturing [21]. The dominating process between the two is largely decided by particle sizes. In Fig. 3a, the amorphous phase looks like a result of cold-welding, which indicates that very fine particles had been once obtained but were cold welded afterward. In comparison, samples milled equally 60 h in Fig. 3b–d exhibit flaky and inhomogeneous in size distribution, which implies the outcome of fracturing. However, the obvious agglomeration still suggests the inclination of cold-welding. To conclude, if milling were prolonged, fracturing would continue until finer crystalline is much more common, which is the prerequisite for amorphous phase. In other words, by comparing Fig. 3a–d, Zr apparently decelerated the progress of amorphization. In Fig. 3c, d, where $x = 0.2$, large particles is found and size distribution is more inconsistent than when $x = 0.1$ as well. An EDS analysis was followed to quantify the chemical compositions in different zones. As shown in Table 2, large particle (zone 1 in Fig. 4 as an example) contains generally more Zr than small ones (zone 2 in Fig. 4 as an example). This is yet the other evidence that Zr is counterproductive for the refining process.

Fig. 5a illustrates the bright field TEM image of $Ti_{1.9}Zr_{0.1}Ni$ milled 60 h and the corresponding selected area electron diffraction (SAED) pattern is shown in Fig. 5b. From the bright field TEM image Fig. 5a combining the HRTEM image Fig. 5c, it can be seen that crystallite size is in the range of 4–10 nm, which is in agreement with estimation using the XRD data (5 nm). The Debye-scherrer rings are indexed according to the interplanar distances. (200) with $d = 1.538$ Å and (110) with $d = 2.170$ Å reflections were found as originated from (Ti, Zr)Ni (space group *Pm3m*). By comparing them with the parameters of TiNi in space group *Pm3m*, an increase of d ((200) with $d = 1.496$ Å and (110) with $d = 2.111$ Å from PDF card 18-0899) is found again, which is ascribed to the increase of lattice constant a as the result of Zr substitution for Ti. These results obtained from TEM investigation are consistent with the analysis by XRD.

3.2. *Electrochemical hydrogen storage properties*

Fig. 6 shows the discharge capacities for Ti_2Ni mechanically alloyed by ball milling 20 h, 40 h, and 60 h respectively as a function of cycle number (at current density of 40 mA/g). Two

Table 2 – Quantitative analysis on the element compositions of different zones.

Spectrum	Content (at%)		
	Ti	Ni	Zr
Zone 1 (with a large particle)	61.07	33.37	5.56
Zone 2 (with fine particles)	61.51	34.52	3.97

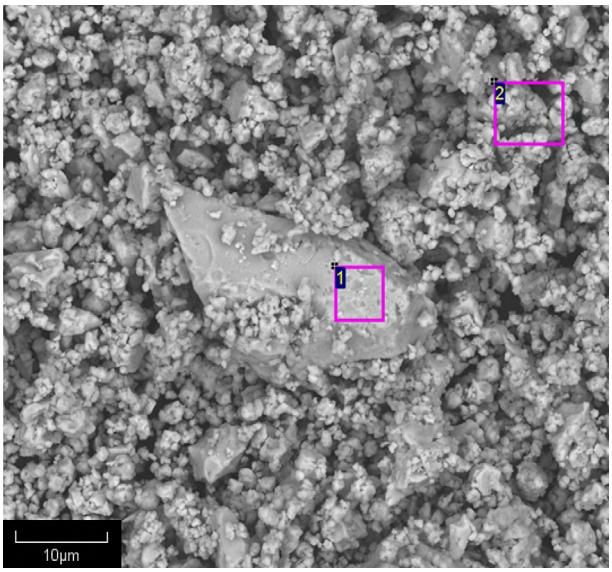

Fig. 4 – SEM with EDS analysis focusing on different zones.

characteristics can be concluded from the curve. First, the discharge capacities apparently increase with milling time. This seems to contradict to Zhao et al.'s result [19], in which longer milling time decreases the discharge capacities of the alloy. However, the difference is in that they ball milled the Ti_2Ni synthesized by solid-state sintering, while our samples were alloyed by ball milling from elemental powders. Longer milling time means more content of alloy produced. In Fig. 1, Ti and Ni peaks are discernible for both (a) (milled 20 h) and (b) (milled 40 h). This denotes incomplete alloying. However, 40 h milled sample obtained more alloy since its element peaks are vague and weaker than the ones milled 20 h. Second, the mechanical alloyed Ti_2Ni exhibits prominent cycling stability and excellent activation properties. The samples milled 20 h and 60 h hardly need activation to attain their stable discharge capacities except for the sample milled 40 h, which was activated immediately after the first cycle. In other words, the mechanical alloyed Ti_2Ni exhibits outstanding electrochemical kinetics. The result is consistent with the one from Zhao et al. [19], in which the amorphous Ti_2Ni had good electrochemical kinetics and steady cycling stability. The advantage of amorphous Ti_2Ni is ascribed to greater surface area provided by ball milling. However, it should be noted that the maximum discharge capacities are not as high as the Ti_2Ni alloyed by the as-sintered sample (278 mAh/g in the first cycle)

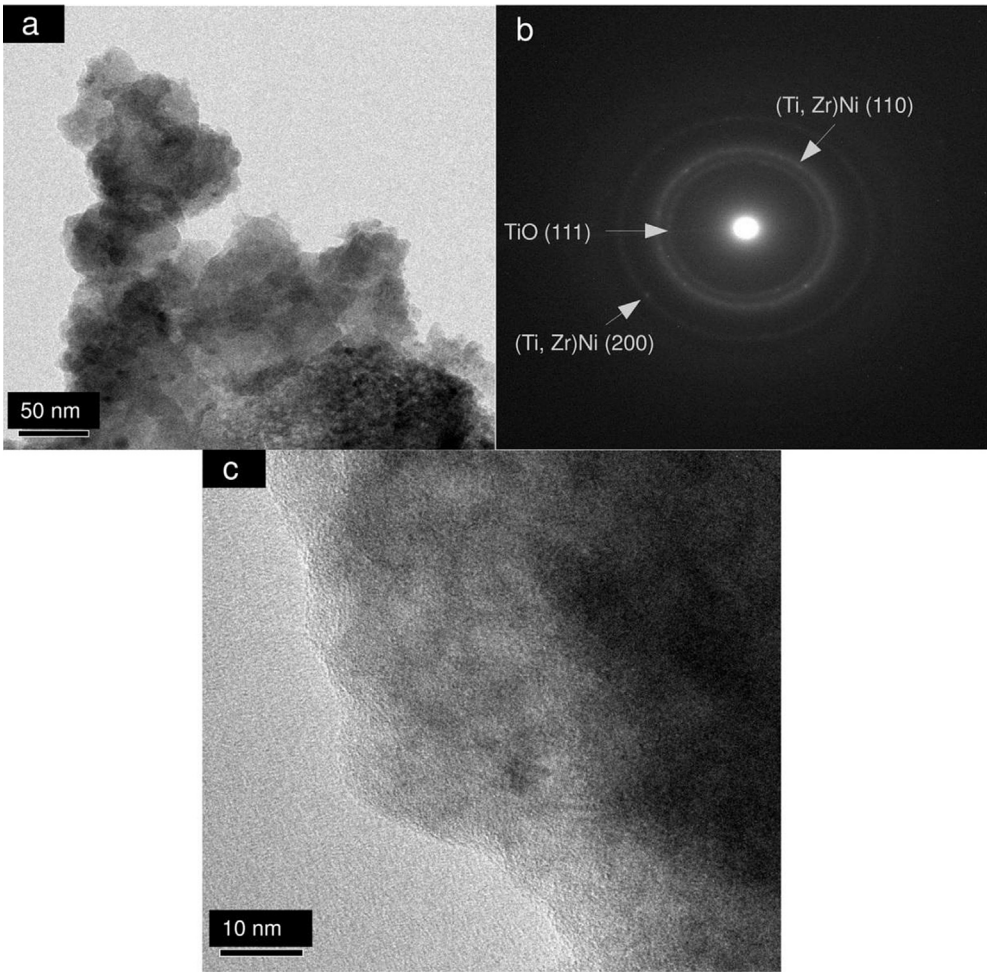

Fig. 5 – TEM micrographs of $Ti_{1.9}Zr_{0.1}Ni$: (a) bright field TEM image, (b) corresponding SAED pattern, and (c) HRTEM image.

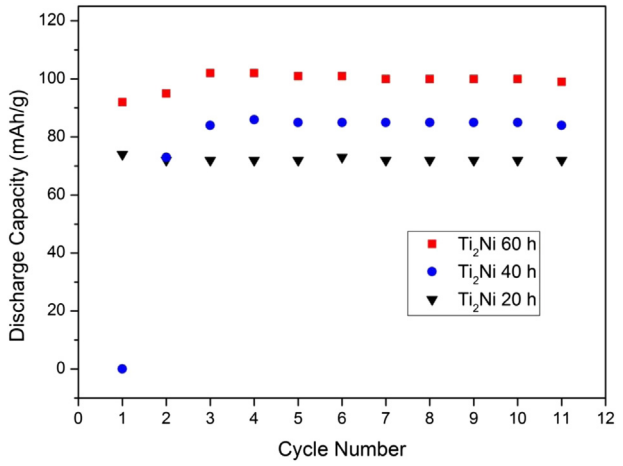

Fig. 6 – Cycling stabilities of Ti_2Ni alloy milled 20 h, 40 h, and 60 h.

[5], which unfortunately has the problem of severe capacities loss during cycling. These evidences suggest that the capacity loss of Ti_2Ni is not caused by the formation of irreversible $Ti_2NiH_{0.5}$ as Luan et al. [4] concluded. The good electrochemical kinetic but lower initial capacity are attributed to the structure of amorphous Ti_2Ni that provides efficient paths for the transportation of hydrogen, while it is in lack of storage sites for hydrogen compared with as-sintered Ti_2Ni.

Fig. 7 compares the cycling discharge capacities of $Ti_{2-x}Zr_xNi$ ($x = 0$, 0.1, 0.2) with a fixed milling time of 60 h. Substantial decrease in discharge capacities occurred when Zr is added to the binary Ti–Ni system, but the cycling stability remains in good shape. As shown in Table 3, the retaining rate for $Ti_{1.8}Zr_{0.2}Ni$ reaches as high as 100%, and the small standard deviation figure suggests considerable steady discharge capacity in the cycling test (capacity retaining rate calculated as introduced in Ref. [23]. $R_h = C_n/C_{max} \times 100\%$). Note that despite decrease of capacity as Zr is introduced, when x increases from 0.1 to 0.2, the discharge capacity increases again in general. From the XRD pattern in Fig. 2, it can be seen that

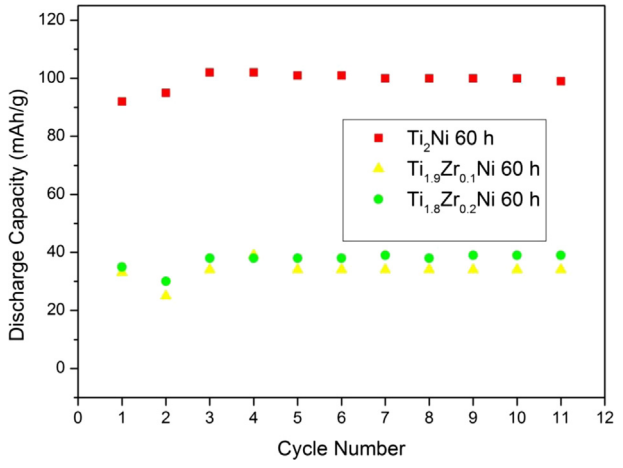

Fig. 7 – Cycling stabilities of $Ti_{2-x}Zr_xNi$ ($x = 0$, 0.1, 0.2) milled 60 h.

Table 3 – Cycling stabilities for $Ti_{2-x}Zr_xNi$ with different milling time and content of Zr.

Milling time (h)	20	40	60		
C_{max} (mAh/g)	74	86	102	39	39
Retaining rate (R_{11})	97.3%	97.7%	97.1%	87.2%	100%
Standard deviation (mAh/g)	0.6	25.5	3.1	3.2	2.7
Content of Zr	$x = 0$			$x = 0.1$	$x = 0.2$

austenitic (Ti, Zr)Ni is the only phase that serves as the hydrogen carrier. Moreover, it is reported that $Ti_{50-x}Zr_xNi_{50}$ has merely a maximum discharge capacity of 85 mAh/g at a discharging rate of C/10 (8.5 mA/g), but it does not suffer capacity loss in cycling [22]. Therefore, the steady performance in cycling for (Ti, Zr)Ni is expected. It could be inferred that the amount of oxidized titanium is significant, since the initial ratio of Ti/Ni is 2 but the final product is (Ti, Zr)Ni. This is the other factor accounts for the severe capacity loss. The increase of the discharge capacity (from $x = 0.1$ to $x = 0.2$) indicates that the substitution of Zr for Ti leads to an expansion in the unit-cell-volume.

In summary, all samples for $Ti_{2-x}Zr_xNi$ exhibit outstanding cycling stability. The stability for Ti_2Ni is ascribed to the amorphous phase obtained by mechanical alloying. As for $Ti_{2-x}Zr_xNi$ ($x = 0.1$, 0.2), the electrochemical properties is in fact a reflection of austenitic (Ti, Zr)Ni phase, which is characteristic of stable cycling performance and low discharge capacity.

4. Conclusions

Amorphous Ti_2Ni was realized by 60 h of ball milling from pure elemental powders. Zr substitution decreases the stability of the amorphous phase of Ti_2Ni, meaning that the threshold of amorphization of Ti_2Ni increases with the presence of Zr. SEM micrographs show that the morphology of amorphous Ti_2Ni milled 60 h is homogenous, whereas with addition of Zr, the particles became flaky and inhomogeneous in size distribution. Fine particles were obtained with addition of Zr (4–5 nm in average), but massive agglomeration was observed. The amorphization process was hindered by additional Zr. Both amorphous Ti_2Ni and austenitic (Ti, Zr)Ni exhibit appealing stable cycling performances. The amorphous Ti_2Ni by ball milling 60 h reached a maximum discharge capacity of 102 mAh/g at a current density of 40 mA/g under room temperature. With Zr substitution, the products were austenitic structure of (Ti, Zr)Ni (with TiO). There is a substantial capacity loss due to the poor performance of austenitic (Ti, Zr)Ni and oxidation of Ti. On one hand, Zr increases the discharge capacity because of the expansion of unit-cell. On the other hand, Ti–Zr–Ni system suffers severe oxidation when synthesized by mechanical alloying. It is found that Zr acts as catalyst to the Ti oxidation reaction. Therefore, it is crucial to develop a new methodology in order to prevent severe oxidation in the case of mechanical alloying Ti–Zr–Ni from elemental powders, until then it may be possible to obtain amorphous phase of $Ti_{2-x}Zr_xNi$.

Acknowledgments

This work is supported by China Scholarship Council (China) and UTBM (France) in the framework of UT-INSA project. The authors would like to thank Dr. A. Lamraoui (LERMPS, UTBM, France), and V. Moutarlier (Institut UTINAM, UMR 6213, France) for their technical assistance concerning SEM and XRD experiments.

REFERENCES

[1] Wang CS, Lei YQ, Wang QD. Effects of Nb and Pd on the electrochemical properties of a Ti–Ni hydrogen-storage electrode. J Power Sources 1998;70:222–7.
[2] Szajek A, Makowiecka M, Jankowska E, Jurczyk M. Electrochemical and electronic properties of nanocrystalline $TiNi_{1-x}M_x$ (M = Mg, Mn, Zr; $x = 0$, 0.125, 0.25) ternary alloys. J Alloys Compd 2005;403:323–8.
[3] Buchner H, Gutjahr MA, Beccu KD, Saufferer H. Wasserstoff in intermetallischen Phasen am Beispiel des Systems Titan-Nickel-Wasserstoff. Z Metalkunde 1972;63:497–500.
[4] Luan B, Cui N, Zhao H, Liu HK, Dou SX. Mechanism of early capacity loss of Ti_2Ni hydrogen-storage alloy electrode. J Power Sources 1995;55:101–6.
[5] Zhao X, Ma L, Yao Y, Ding Y, Shen X. Ti_2Ni alloy: a potential candidate for hydrogen storage in nickel/metal hydride secondary batteries. Energy Environ. Sci. 2010;3:1316–21.
[6] Luan B, Cui N, Zhao H, Zhong S, Liu HK, Dou SX. Studies on the performance of $Ti_2Ni_{1-x}Al_x$ hydrogen storage alloy electrodes. J Alloys Compd 1996;233:225–30.
[7] Luan B, Cui N, Zhao HJ, Liu HK, Dou SX. Effects of potassium-boron addition on the performance of titanium based hydrogen storage alloy electrodes. Int J Hydrogen Energy 1996;21:373–9.
[8] Takeshita HT, Tanaka H, Kiyobayashi T, Takeichi N, Kuriyama N. Hydrogenation characteristics of Ti_2Ni and Ti_4Ni_2X (X = O, N, C). J Alloys Compd 2002;330–332:517–21.
[9] Hu W, Wang J, Wang L, Wu Y, Wang L. Electrochemical hydrogen storage in $(Ti_{1-x}V_x)_2Ni$ ($x = 0.05$–0.3) alloys comprising icosahedral quasicrystalline phase. Electrochim Acta 2009;54:2770–3.
[10] Cuevas F, Latroche M, Bourée-Vigneron F, Percheron-Guégan A. A conjoint XRD–ND analysis of the crystal structures of austenitic and martensitic $Ti_{0.64}Zr_{0.36}Ni$ hydrides. J Solid State Chem 2006;179:3295–307.
[11] Guiose B, Cuevas F, Décamps B, Percheron-Guégan A. Solid–gas and electrochemical hydrogenation properties of pseudo-binary (Ti, Zr)Ni intermetallic compounds. Int J Hydrogen Energy 2008;33:5795–800.
[12] Guiose B, Cuevas F, Décamps B, Leroy E, Percheron-Guégan A. Microstructural analysis of the ageing of pseudo-binary (Ti, Zr)Ni intermetallic compounds as negative electrodes of Ni-MH batteries. Electrochim Acta 2009;54:2781–9.
[13] Lee GW, Gangopadhyay AK, Kelton KF. Phase diagram studies of Ti–Zr–Ni alloys containing less than 40 at.% Ni and estimated critical cooling rate for icosahedral quasicrystal formation from the liquid. Acta Mater 2011;59:4964–73.
[14] Buhrer W, Gotthardt R, Kulik A, Mercier O, Staub F. Powder neutron diffraction study of nickel–titanium martensite. Journal of Physics F: Metal Physics 1983;13:L77–81.
[15] Kudoh Y, Tokonami M, Miyazaki S, Otsuka K. Crystal structure of the martensite in Ti-49.2 at.%Ni alloy analyzed by the single crystal X-ray diffraction method. Acta Metallurgica 1985;33:2049–56.
[16] Cuevas F, Latroche M, Ochin P, Dezellus A, Fernández J, Sánchez C, et al. Influence of the martensitic transformation on the hydrogenation properties of $Ti_{50-x}Zr_xNi_{50}$ alloys. J Alloys Compd 2002;330–332:250–5.
[17] Cuevas F, Latroche M, Percheron-Guégan A. Relationship between polymorphism and hydrogenation properties in $Ti_{0.64}Zr_{0.36}Ni$ alloy. J Alloys Compd 2005;404–406:545–9.
[18] Zhao X, Ma L, Qu X, Ding Y, Shen X. Effect of mechanical milling on the structure and electrochemical properties of Ti_2Ni alloy in an alkaline battery. Energy Fuels 2009;23:4678–82.
[19] Zhao X, Zhou J, Shen X, Yang M, Ma L. Structure and electrochemical hydrogen storage properties of A_2B-type Ti–Zr–Ni alloys. Int J Hydrogen Energy 2012;37:5050–5.
[20] Tria S, Elkedim O, Hamzaoui R, Guo X, Bernard F, Millot N, et al. Deposition and characterization of cold sprayed nanocrystalline NiTi. Powder Technol 2011;210:181–8.
[21] Suryanarayana C. Mechanical alloying and milling. Prog Mater Sci 2001;46:1–184.
[22] Cuevas F, Latroche M, Ochin P, Dezellus A, Percheron-Guégan A. Influence of polymorphism on the electrochemical properties of $(Ti_{0.64}Zr_{0.36})Ni$ alloys. J Alloys Compd 2003;356–357:730–3.
[23] Zhang Y, Ren H, Li B, Guo S, Pang Z, Wang X. Electrochemical hydrogen storage characteristics of nanocrystalline and amorphous $Mg_{20}Ni_{10-x}Co_x$ ($x = 0$–4) alloys prepared by melt spinning. Int J Hydrogen Energy 2009;34:8144–51.